Separating function from structure in perfusion imaging of the aging brain

Iris Asllani[1],[*], **Christian Habeck**[2], **Ajna Borogovac**[3], **Truman R. Brown**[1],[3], **Adam M. Brickman**[2], and **Yaakov Stern**[2]

[1]Program for Imaging & Cognitive Sciences in the Department of Radiology, 710 West 168th Street, Columbia University, New York, NY, 10032

[2]The Cognitive Neuroscience Division of the Taub Institute for Research on Alzheimer's Disease and the Aging of the Brain, 710 West 168th Street, Columbia University, New York, NY, 10032

[3]Department of Biomedical Engineering, 710 West 168th Street, Columbia University, New York, NY, 10032

Abstract

The accuracy of the cerebral blood flow (CBF) imaging methods in humans has been impeded by the partial volume effects (PVE), which are a consequence of the limited spatial resolution. Because of brain atrophy, PVE can be particularly problematic in imaging the elderly and can considerably overestimate the CBF difference with the young. The primary goal of this study was to separate the structural decline from the true CBF reduction in elderly. To this end, a PVE-correction algorithm was applied on the CBF images acquired with spin-echo EPI continuous arterial spin labeling MRI (voxel size = $3.4 \times 3.4 \times 8$ mm^3). Tissue-specific CBF images that were independent of voxels' tissue fractional volume were obtained in elderly (N = 30) and young (N = 26); mean age difference was 43 years. Globally, PVE-corrected gray matter CBF was 88.2 ± 16.1 and 107.3 ± 17.5 mL/100g min in elderly and young, respectively. The largest PVE contribution was found in the frontal lobe and accounted for an additional 10% and 12% increase in the age-related CBF difference between men and women, respectively. The GM-to-WM CBF ratios were found to be on average 3.5 in elderly and 3.9 in young. Whole brain voxelwise comparisons showed marked CBF decrease in anterior cingulate (bilateral), caudate (bilateral), cingulate gyrus (bilateral), cuneus (left), inferior frontal gyrus (left), insula (left), middle frontal gyrus (left), precuneus (bilateral), prefrontal cortex (bilateral), superior frontal gyrus (bilateral) in men and amygdala (bilateral), hypothalamus (left), hippocampus (bilateral), and middle frontal gyrus (right) in women.

Keywords

aging; arterial spin labeling (ASL); brain atrophy; cerebral blood flow (CBF); partial volume effects (PVE); perfusion MRI

INTRODUCTION

Imaging techniques such as MRI, PET, and SPECT are commonly employed to investigate changes in cerebral blood flow (CBF) and metabolism associated with normal aging. However, a major source of error in these techniques is the partial volume effects (PVE), which are a consequence of the limited spatial resolution in routine human brain imaging. A

[*]Corresponding author phone: 212 342 0183, fax: 212 342 5773, e-mail: ia2026@columbia.edu.

typical voxel in functional imaging with MRI and nuclear medicine techniques is around or larger than 60 mm^3 and as such, it usually contains a mixture of gray matter (GM), white matter (WM), and CSF tissues. Therefore, the acquired signal reflects a volume-averaged contribution from all the tissues and cannot distinguish voxel's GM from WM and/or CSF. It follows that the larger the voxel size, the more heterogeneous the voxel hence the more severe the PVE. In a routine arterial spin labeling (ASL) perfusion MRI experiment, the measured CBF values can be substantially under-estimated even for voxels with 80% or higher GM content (Asllani, et al. 2008a).

Because of tissue atrophy, PVE can be particularly problematic in studies of elderly, where thinning of the cortex and the consequent contamination of GM voxels by WM and CSF increase voxel heterogeneity (Kohn, et al. 1991; Tanna, et al. 1991). Failure to correct for this dilution effect could potentially yield a difference between young and elderly even in the absence of a *true* perfusion decline.

Although the substantial error introduced by PVE in estimating CBF in elderly has been long acknowledged (Martin, et al. 1991; Meltzer, et al. 2000; Tanna, et al. 1991), only few PET studies have attempted to correct for them (Relihac 2001) and no correction has been done in ASL perfusion imaging. While ASL MRI offers several advantages over PET (Barbier, et al. 2001), its signal dependency on PVE is more complex because the measured signal is a ratio of two images, each of which is affected by voxel heterogeneity (Asllani, et al. 2008a).

Kwong et al. predicted large deviations of CBF values in voxels with CSF content of $\geq 50\%$ for pulsed ASL (Kwong, et al. 1995) and suggested that ΔT_1 maps can be qualitatively used to counteract the impact of PVE due to CSF. Simulated data reported by Wiersma et al. for flow-sensitive alternating inversion recovery (FAIR) ASL have shown that for voxels with CSF content 0–40% CBF can be overestimated by up to 50%; for higher CSF percentages, the errors were found to increase steeply (Wiersma, et al. 2006). Taking the magnitude of the FAIR signal proved to be quite effective for voxels with CSF content 0–40% (Wiersma, et al. 2006). These studies address the effect of CSF signal in pulsed ASL that results from a discrepancy between zero-crossing inversion times and arterial transit times. As such, they are particular to pulsed ASL and not directly applicable to continuous ASL. Furthermore, no attempt was made by these studies to correct for the partial volume effects of WM.

Generally, the problem of PVE is circumvented by trying to include only voxels with high GM content. To this end, posterior probability masks obtained from high resolution MRI are used and a given voxel is considered GM if its P[GM] is larger than a threshold value, commonly chosen to be 0.8 (Asllani, et al. 2008c; Johnson, et al. 2005) or 0.7 (Noth, et al. 2006). In some cases, T_1 images are acquired and a given voxel is deemed GM if its T_1 value falls within the *a priori* chosen range (Parkes, et al. 2004). However, even for voxels with GM content $\geq 80\%$, the PVE can cause an underestimation of CBF by as much as 24% (Asllani, et al. 2008a). Furthermore, these exclusion criteria make the comparison between age groups difficult as many voxels that would survive the threshold for young subjects, would be missed in elderly where cortical thinning due to atrophy can be quite substantial (Schmidt and Sokoloff 2001)

Recently, an algorithm that corrects for PVE in ASL MRI has been developed (Asllani, et al. 2008a). The algorithm is based on linear regression and estimates the pure tissue signals by modeling the intensity of a given voxel as a weighted sum of tissue specific contributions with the weighting coefficients being the tissue's fractional volumes (Asllani, et al. 2008a).

The primary goal of this study was to apply the PVE correction algorithm to the ASL CBF baseline data from young and elderly in order to separate structural changes due to normal

aging from those due to a 'true' CBF decline associated with it. As exploratory goals, the effects of gender and brain laterality were also investigated.

METHODS

Participants

Baseline continuous ASL (CASL) CBF images were acquired from two groups: healthy elderly (HE), [N = 30, mean age = 69 ± 6 y, age range = (62–86), 16 men (53.1%, mean age = 69.2 ± 5.6), 14 women (46.9 %, mean age 68.0 ± 6.2)], and healthy young (HY), [N = 26, mean age = 26 ± 3 y, age range = (21–31), 8 men (35.7%, mean age = 26.4 ± 2.9) and 18 women (64.3%, mean age = 26.2 ± 3.2.), menstrual cycle was not controlled for]. All participants were right handed.

Within each group, men and women did not differ in age (HY: $t = 0.12$, p = 0.91; HE: $t = 0.55$, p = 0.59). By self-report and interview, participants did not have past or current history of medical, neurological, or psychiatric disorders or treatment with psychoactive medication. Participants were screened for dementia with interview and psychometric assessment; none met the diagnostic criteria. HE subjects were part of an Alzheimer's disease study previously reported (Asllani, et al. 2008c).

Image acquisition

For each participant, 30 CASL SE-EPI labeled/control pairs and a high resolution T_1-weighted, 3D spoiled gradient (SPGR), were acquired on a 1.5 T Philips Intera scanner. CASL images were acquired as described in (Asllani, et al. 2008b) with: labeling duration = 2000 ms, post-labeling delay (PLD) = 800 ms, TE/TR = 35 ms/5000 ms, flip angle = 90°, FOV = 220 × 192.5 mm^2, in-plane resolution = 3.4 × 3.4 mm^2, slice thickness/gap = 8.0 mm/1.0 mm, number of axial slices = 15. Slices were acquired in ascending mode with slice acquisition time = 64 ms, which set the effective PLD in the [800 – 1696] ms range.

SPGR was acquired with: TE/TR = 3 ms/34 ms, flip angle = 45°, acquisition matrix = 256 × 256 × 124, voxel size = 0.94 × 0.94 × 1.29 mm^3.

Image Processing and CBF computation

Preprocessing—was implemented using SPM5 software as previously described (Asllani, et al. 2008c). Briefly, for each subject, images were preprocessed as follows: (1) all EPI images were realigned to the first acquired. (2) GM, WM, and CSF posterior probability images were obtained from subject's SPGR. (3) The SPGR and posterior probability maps were co-registered to the first acquired EPI and used to represent the fractional tissue volume at each voxel.

PVE-correction—A detailed treatment of the underlying theory and methodology of the PVE correction algorithm is given in (Asllani, et al. 2008a). Briefly, for each subject, the linear regression algorithm estimates: (1) the magnetization values, m_{GM}, m_{WM}, m_{CSF} using subject's mean control SE-EPI image, and (2) the ASL difference values, δm_{GM} and δm_{WM}, using the mean (control-label) difference image.

For each subject, linear regression was performed in subject's native space using a regression kernel of 11×11×1 voxels and following the procedure described in (Asllani, et al. 2008a).

CBF computation—As described in detail in (Asllani, et al. 2008a), for each subject, fractional signal images obtained from the regression algorithm were used to compute tissue specific CBF images, *f*, also referred to as 'flow density' images:

$$f_{GM} = (\frac{\delta m_{GM}}{m_{GM}}) \cdot F_{GM}$$

<div align="right">Eq. [1]</div>

and

$$f_{WM} = (\frac{\delta m_{WM}}{m_{WM}}) \cdot F_{WM}$$

<div align="right">Eq. [2]</div>

, where $F_{tissue} = \frac{\lambda}{2\alpha} \left\{ \begin{matrix} T_{1a} \left[e^{(\min(\delta a - \omega, 0) - \delta a)/T_{1a}} - e^{(\min[\delta - w, 0] - \delta)/T_{1a}} \right] + \\ e^{-\delta/T_{1a}} \left[T_{1s} e^{-\omega/T_{1ns}} (1 - e^{\min[\delta - \tau, 0]/T_{1s}}) + T_1 (e^{\min[\delta - \omega, 0]/T_{1ns}} - e^{-\omega/T_{1ns}}) \right] \end{matrix} \right\}^{-1}$ in accordance with the two-compartment model (Wang, et al. 2002).

The following parameter values were used to compute CBF: longitudinal relaxation, (T_1) of blood = 1400 ms; blood/tissue water partition = 0.9 mL/g; transit time = 1300 ms; labeling duration = 2000 ms; tissue T_1 in absence of RF = 1150 ms and 800 ms for GM and WM, respectively; T_1 in presence of RF = 750 ms and 530 ms for GM and WM, respectively (Alsop and Detre 1996); PLD adjusted to account for the inter-slice acquisition time, *PLDs* = (acquisition slice −1) (64 ms) + 800 ms; labeling efficiency for CASL at 1.5T on Philips Intera = 0.70 (Werner, et al. 2005).

Partial flow images, f^P, which account for the tissue fractional volume and are, therefore, also referred to as fractional tissue CBF images, were computed as:

$$f_{GM}^P = P_{GM} \cdot (\frac{\delta m_{GM}}{m_{GM}}) \cdot F_{GM}$$

<div align="right">Eq. [3]</div>

$$f_{WM}^P = P_{WM} \cdot (\frac{\delta m_{WM}}{m_{WM}}) \cdot F_{WM}$$

<div align="right">Eq. [4]</div>

where P_{GM} and P_{WM} represent the GM and WM fractional volumes, respectively.

Net CBF was computed as sum of partial flow contributions:

$$f_{NET} = f_{GM}^P + f_{WM}^P$$

<div align="right">Eq. [5]</div>

Ratios of f_{GM}/f_{WM} were also computed for each subject.

Data Analysis

To test the validity of the PVE-correction algorithm, for each subject, 5 test-ROIs were obtained by including voxels with GM content varying as: 0<P[GM]<0.2, 0.2<P[GM]<0.4, 0.4<P[GM]<0.6, 0.6<P[GM]<0.8, 0.8<P[GM]<1.0 using subject's GM posterior probability image. GM CBF values for corrected and uncorrected data from these test-ROIs are

reported. It is important to note that these ROIs are not 'functional' regions in the conventional sense and may include voxels not adjacent to each other, which is the reason we refer to them as test-ROIs so that to distinguish them from the functional ROIs described below.

ROI analysis—For each subject, a whole brain GM ROI was obtained by including only voxels with GM content of $\geq 80\%$. Furthermore, group mean CBF values were obtained for left and right hemispheres, on the four major lobes: Frontal Lobe (FL), Parietal Lobe (PL), Occipital Lobe (OL), and Temporal Lobe (TL) using wfu_pickatlas (Maldjian, et al. 2003). All global and lobe-wise ROIs satisfied the statistical power requirement of ≥ 0.8 (effect size = 15 mL/(100g min), $\alpha_{\text{two-tailed}}=0.05$ per ROI) as computed from an independent sample of healthy elderly population (Asllani, et al. 2008b).

To avoid bias in the analysis and ensure that the same voxels were analyzed in CBF images from both age-groups, a 'template' GM mask was made by conjoining all the posterior probability GM maps of HY participants with the condition that only voxels for which at least 10 subjects satisfied the criterion P[GM]>0.8 were included. All the ROIs that were used in the analysis were conjoined with this mask prior to extracting its value from the individual CBF images.

Histograms of the ratios of ${f_{GM}}/{f_{WM}}$ were computed for each lobe and averaged across subjects. For each subject, only voxels with ratio values between 0 and 3 standard deviations (s.d.) away from the mean were included for group comparisons.

Statistical Analysis—ROI-wise between-group (HE *vs.* HY) differences in CBF were examined by multiple regression of summed values of GM CBF in a given ROI as the independent variable and age and gender as regressors (F statistics were set at P<0.05).

Once a significant gender effect was established, the age group CBF differences in the left and right lobe ROIs were tested for women and men separately using a two_tailed t-test (α=0.05).

Voxelwise Analysis—To map regions in the brain with a significant age-effect in CBF, the (HE - HY) CBF contrast was run for men and women, separately. The within-gender comparisons were computed using fixed effect model based on the algorithm provided by SPM5. The analysis accounted for the 'unbalanced' sample sizes and corrected for multiple comparisons at a cluster level of 50 voxels resulting in a threshold T-value = 3.84 (P < 0.005). Only voxels contained in the conjunction of all individual SE-EPI masks were analyzed.

RESULTS

PVE-correction yielded flow density maps independent of voxels' heterogeneity

The novelty of the PVE-correction methods is that for each subject it yields tissue-specific 'flow density' images. Assuming that for a given person, GM and WM 'flow densities' do not vary substantially across the brain, one would expect the spatial distributions of these *pure* flow maps to be relatively homogenous. This expectation is qualitatively borne out in Fig.1 where group averages of flow density images f_{GM} (1st row) and f_{WM} (3rd row), computed as per Eq.[1] & Eq [2], are shown in Figs.1A & 1B for HY and HE, respectively; 2nd and 4th rows show fractional CBF images, f_{GM}^{P} and f_{WM}^{P}, respectively, which were computed as per Eq. [3] & Eq [4] and account for the partial volume of each tissue at a given voxel; the last row shows net CBF images (Eq.[5]).

Theoretically, the value at each voxel in a tissue-specific flow density image represents the amount of flow the voxel would have if it were entirely comprised of that tissue. It follows that for a given tissue, PVE-corrected pure CBF image should be independent of voxel's content of that tissue. As proof of concept, we obtained f_{GM} values from voxels varying in GM content from 0–100%, step of 20%, and compared them with values from data uncorrected for PVE. Results are shown in Figs.2A & 2B for HE and HY, respectively. As predicted, the PVE-corrected data were independent of voxels' GM content – the flow density values for voxels with (0–20)% GM were similar to those with GM content > 80% whereas the PVE-uncorrected CBF values varied with voxels' heterogeneity. Furthermore, even for voxels with P[GM]>0.8, the uncorrected method underestimated the net CBF by 16% and 13% in HE and HY, respectively, as compared to the PVE-correction method.

Fig.2 makes two additional and important points: First, GM flow density for HE is lower than that of HY. Second, although PVE are present in both groups, they affect HE more than the HY, which was expected given the presence of atrophy in the elderly. In fact, the number of ($2\times2\times2$ mm^3) MNI voxels with GM content > 80% was 67405 in HE vs. 83075 in HY, implying an overall 19% percent decrease in global GM volume in elderly. We investigate these points in some quantitative detail in the following sections.

PVE and gender had a significant effect in GM CBF difference between elderly and young

Globally, f_{GM} was ~18 % lower in HE compared to HY (88.2 ± 16.1 *vs.* 107.3 ± 17.5 mL/ 100g min) with age and gender accounting for 48% of the variance [$F(2,56) = 8.1$, P<0.0008]. However, when GM partial volume differences between the two age groups were included, f_{GM}^{P} in HE was ~30% lower than in HY, (61.0 ± 10.2 mL/100g•min *vs.* 87.6 ± 14.4) thus contributing an additional 12 % in the observed global difference. In this case, age and gender accounted for 62% of the observed variability in [$F(2,56)= 18.7$, P< 0.00001]. Gender alone accounted for 30% and 37% of the variance in f_{GM} and f_{GM}^{P} data, respectively, (P<0.01 in both cases). Henceforth, we report on regional specificity and the effects of age, atrophy, and laterality for women and men, separately.

Age-related CBF decline was larger in men

Figs.3A & 3B show lobewise average values of f_{GM} (solid) and f_{GM}^{P} (striped) for women and men, respectively. Men (Fig.3B) were more affected by age than women; in all the lobes both density, (f_{GM}), and fractional, (f_{GM}^{P}), flow were significantly lower in HE males as compared to their young counterpart (p < 0.001 for all, $\alpha_{one-tailed} = 0.05$). For f_{GM}, the largest difference (~30%) between HY and HE men was found in the frontal and parietal lobes, followed by the temporal and occipital lobes with 16% and 15%, respectively. Even when only voxels with GM content ≥80% were included, PVE accounted for an additional 9% difference between young and elderly in the frontal lobe, followed by an average of ~ 7% in the other lobes (Fig. 3B, striped columns).

For females, (Fig.3A), the largest (HY-HE) difference in f_{GM} was found in the occipital lobe (~ 8%) followed by the frontal (~ 7%) and temporal lobes (~6%). These differences, however, did not reach statistical significance in any of the lobes (p > 0.17, $\alpha_{one-tailed} = 0.05$, for all.) But, when GM atrophy was accounted for (by including the variability in fractional volume content in voxels with P[GM]>0.8 between the two age groups, Fig.3A - striped columns), the differences were found to be significant with the largest observed in the frontal lobe (17 %), followed by the occipital (16%), temporal (15%), and parietal (12%) lobes, (p > 0. 05 for all).

GM CBF decline due to aging was region-and gender-specific

Figs.4A & 4B show SPM{T }maps of the (HY-HE) contrasts for f_{GM} (red) and f_{NET} (green) overlaid on a surface rendering of the brain for females and males, respectively; the overlap between the two contrasts is shown in orange. As expected, the T-map for net CBF yielded larger and more globalized areas of contrast between HY and HE because, in addition to pure flow differences, it also includes the structural variability between the two age groups.

In men, areas in f_{GM} that survived the statistical threshold for the age difference contrast included: anterior cingulate (bilateral), caudate (bilateral), cingulate gyrus (bilateral), cuneus (left), inferior frontal gyrus (left), insula (left), middle frontal gyrus (left), precuneus (bilateral), prefrontal cortex (bilateral), superior frontal gyrus (bilateral). In women, those areas were: amygdala (bilateral), hypothalamus (left), hippocampus (bilateral), and middle frontal gyrus (right).

The flow decline but not atrophy was asymmetric in both men and women

Both men and women showed a substantial laterality effect in GM flow density changes related to aging (Fig. 4, areas in red). However, the spatial distribution of the observed asymmetry was gender specific with men showing more areas of reduced GM CBF in the left hemisphere than in the right. The following regions had ~ 50% more voxels that survived the statistical threshold in the left hemisphere as compared to the right: anterior cingulate, caudate, cuneus, inferior frontal gyrus, inferior temporal gyrus, insula, lingual gyrus, middle frontal gyrus, prefrontal cortex, frontal lobe, and occipital lobe. For women, the frontal and parietal cortical areas showed more GM CBF decline in the right hemisphere as compared to the left.

When atrophy was accounted for (Fig. 4, areas in green), the age contrast maps were relatively symmetrical implying a similar rate of atrophy in both hemispheres.

Voxelwise global differences in ratios of f_{GM}/f_{WM} were slightly lower in HE

Histograms for the brain-wise ratios of f_{GM}/f_{WM} in each age group are shown in Figs.4A & 4B for females and males, respectively. For both men and women, the global values for the ratio of f_{GM}/f_{WM} were ~ 3.5 and ~3.9 for HE and HY, respectively; the differences did not reach statistical significance for either gender group.

DISCUSSION

This is the first study to provide a measurement of CBF that is independent of voxels' heterogeneity and that accounts for variability in tissue fractional volumes between elderly and young populations. This was achieved by applying a linear regression algorithm that corrects for PVE in ASL perfusion images (Asllani, et al. 2008a). Our primary findings, summarized in Fig.1&Fig 2, indicate a global age-related decrease in GM CBF of ~ 15%, which is substantially lower than what has been previously reported for ASL (~ 30% by Ances et al. and Restom et al. (Ances, et al. 2008; Restom, et al. 2007), and ~ 20% by Parkes et al. (Parkes, et al. 2004)). When including the contribution of PVE in voxels with GM content ≥ 80%, the observed age-related CBF difference was ~30%, in good agreement with Ances et al. and Restom et al. studies. The gender and laterality effects in GM CBF found here were similar to those reported by Parkes et al. (Parkes, et al. 2004) although a direct quantitative comparison is not straightforward.

Several functional activation studies have shown that even in the absence of Alzheimer's disease and other degenerative illnesses, aging is accompanied by significant declines in function related to memory, language, face/object recognition, and tasks that require higher level of visuospatial processing (Beason-Held, et al. 2008a; Beason-Held, et al. 2008b; Hazlett, et al. 1998; Miller, et al. 2008; Stern, et al. 2008). However, a quantitative assessment of these functional impairments has been lacking as the observed changes are typically expressed in relative terms and baseline values are not obtained. The effect of baseline variability in BOLD fMRI data was experimentally shown in a study by Brown et al., where a 20% increase in baseline CBF following the intake of acetazolamide corresponded to a 35% reduction in the BOLD response in the motor cortex on the same subjects, for the same stimulus (Brown, et al. 2003).

Therefore, a method that yields absolute and accurate measurement of CBF that is uncontaminated by PVE, should prove essential especially in studies of age-related functional decline where conclusions are often based on comparing elderly with young. As shown here, even in voxels with high GM content (>80%), the PVE contribution in CBF measurement are regional and gender specific and may have a considerable contribution to the measured CBF difference between the age groups.

In addition to its relevance for activation studies, separating structure from function in imaging of the aging brain would aid in our understanding of the causality in disease related changes in brain structure and function. Recently, an Alzheimer's disease study by our team showed a disease related covariance pattern derived from CBF ASL measurement that was able to distinguish patients from controls with high specificity and sensitivity at baseline (Asllani, et al. 2008c). Another study by Andrews-Hanna et al. observed an age related large-scale disruption of brain systems by applying functional correlation methods to BOLD fMRI data (Andrews-Hanna, et al. 2007). As typical for functional MRI studies, the spatial resolution in both these studies was relatively low, ~$(3.5 \times 3.5 \times 8 \text{ mm}^3)$, which, especially in elderly, would make the contribution of PVE considerable. However, neither study accounted for additional variance in the data due to inter-and intra-subject variability in PVE. With the new technique presented here, we should now be able to separate the structural from the functional networks in the brain and study their relationship with the disease onset and progression thus increasing the diagnostic potential of MRI.

The advantage of the PVE-correction method developed here is that it yields tissue-specific CBF values and, as such, voxelwise ratios of GM flow to WM flow can be obtained. This ratio can in itself be used as indicative of the severity of atrophy and structural deterioration. Here, we found that the mean values for GM to WM CBF ratios were ~ 3.7, with the values being somewhat higher in young subjects. These ratios were higher than the value measured or assumed in previous perfusion MRI studies (Johnson, et al. 2005; Parkes, et al. 2004; Ye, et al. 2000) but, as expected, they were similar to what has been reported by high-resolution studies as PVE decrease with decreasing voxel size (Donahue, et al. 2006). Visual inspection of the histograms of these ratios, (Fig.5), indicates a wider distribution of values in elderly men, which would be consistent with the finding of a widespread region-specific decline in GM CBF in this group.

Given the relatively low sample sizes in our study, caution should be drawn in interpreting the effect of gender in the observed CBF difference between the two age groups. Various PET studies have examined the gender differences in CBF and metabolism during baseline function and in response to activation (Esposito, et al. 1996; George, et al. 1996; Good, et al. 2001; Gur, et al. 1995; Kawachi, et al. 2002). The findings have been inconsistent and remain controversial. This inconsistency could be due to the dependence of the impact of

PVE on the age difference as well as other factors such as education, weight, or exercise. Future work is needed to investigate the differential gender effect on aging of the brain.

Also, caution should be drawn in interpreting the results presented here from several methodological standpoints. Although we combined a long labeling pulse with a relatively long post-labeling delay to diminish the contamination from the arterial signal, we did not account for any age-related changes in arterial transit times. In a previous study where the same acquisition paradigm was used, a longer post-labeling delay showed no significant difference in measured CBF thus implying that the delay was sufficiently long for the arterial signal not have a significant role in CBF values (Asllani, et al. 2008c). However, it is likely that the results presented here might not reflect an absolute difference in CBF values but a combined effect of lower CBF and longer transit times in elderly.

Second, spatial smoothing is implicit in the application of the regression algorithm – the smoothing effect depends on the regression kernel size (see (Asllani, et al. 2008c) for details). Although spatial smoothing is routine in image analysis of MRI data, more work is needed to estimate its effect on the pure CBF images especially for activation studies where localization of functional activity is very important.

Third, in this study we did not account for other factors such as weight and exercise that could potentially affect the aging brain.

In conclusion, in this study we showed the feasibility of using PVE-corrected ASL perfusion MRI to separate structural changes due to normal aging from those of *true* CBF decline associated with it thereby providing a technique that yields absolute measurement of tissue-specific CBF, which we believe would prove essential in studying of the aging brain.

Acknowledgments

BIBLIOGRAPHY

Alsop DC, Detre JA. Reduced transit-time sensitivity in noninvasive magnetic resonance imaging of human cerebral blood flow. J Cereb Blood Flow Metab. 1996; 16(6):1236–1249. [PubMed: 8898697]

Ances BM, Liang CL, Leontiev O, Perthen JE, Fleisher AS, Lansing AE, Buxton RB. Effects of aging on cerebral blood flow, oxygen metabolism, and blood oxygenation level dependent responses to visual stimulation. Hum Brain Mapp. 2008

Andrews-Hanna JR, Snyder AZ, Vincent JL, Lustig C, Head D, Raichle ME, Buckner RL. Disruption of large-scale brain systems in advanced aging. Neuron. 2007; 56(5):924–935. [PubMed: 18054866]

Asllani I, Borogovac A, Brown T. A Regression Algorithm Correcting for Partial Volume Effects in Arterial Spin Labeling MRI. Magnetic Resonance in Medicine. 2008a in press.

Asllani I, Borogovac A, Wright C, Sacco R, Brown TR, Zarahn E. An investigation of statistical power for continuous arterial spin labeling imaging at 1.5 T. Neuroimage. 2008b; 39(3):1246–1256. [PubMed: 18036834]

Asllani I, Habeck C, Scarmeas N, Borogovac A, Brown TR, Stern Y. Multivariate and univariate analysis of continuous arterial spin labeling perfusion MRI in Alzheimer's disease. J Cereb Blood Flow Metab. 2008c; 28(4):725–736. [PubMed: 17960142]

Barbier EL, Lamalle L, Decorps M. Methodology of brain perfusion imaging. J Magn Reson Imaging. 2001; 13(4):496–520. [PubMed: 11276094]

Beason-Held LL, Kraut MA, Resnick SM. I. Longitudinal changes in aging brain function. Neurobiol Aging. 2008a; 29(4):483–496. [PubMed: 17184881]

Beason-Held LL, Kraut MA, Resnick SM. II. Temporal patterns of longitudinal change in aging brain function. Neurobiol Aging. 2008b; 29(4):497–513. [PubMed: 17178430]

Brown GG, Eyler Zorrilla LT, Georgy B, Kindermann SS, Wong EC, Buxton RB. BOLD and perfusion response to finger-thumb apposition after acetazolamide administration: differential relationship to global perfusion. J Cereb Blood Flow Metab. 2003; 23(7):829–837. [PubMed: 12843786]

Donahue MJ, Lu H, Jones CK, Pekar JJ, van Zijl PC. An account of the discrepancy between MRI and PET cerebral blood flow measures. A high-field MRI investigation. NMR Biomed. 2006; 19(8): 1043–1054. [PubMed: 16948114]

Esposito G, Van Horn JD, Weinberger DR, Berman KF. Gender differences in cerebral blood flow as a function of cognitive state with PET. J Nucl Med. 1996; 37(4):559–564. [PubMed: 8691239]

George MS, Ketter TA, Parekh PI, Herscovitch P, Post RM. Gender differences in regional cerebral blood flow during transient self-induced sadness or happiness. Biol Psychiatry. 1996; 40(9):859–871. [PubMed: 8896772]

Good CD, Johnsrude IS, Ashburner J, Henson RN, Friston KJ, Frackowiak RS. A voxel-based morphometric study of ageing in 465 normal adult human brains. Neuroimage. 2001; 14(1 Pt 1): 21–36. [PubMed: 11525331]

Gur RC, Mozley LH, Mozley PD, Resnick SM, Karp JS, Alavi A, Arnold SE, Gur RE. Sex differences in regional cerebral glucose metabolism during a resting state. Science. 1995; 267(5197):528–531. [PubMed: 7824953]

Hazlett EA, Buchsbaum MS, Mohs RC, Spiegel-Cohen J, Wei TC, Azueta R, Haznedar MM, Singer MB, Shihabuddin L, Luu-Hsia C, et al. Age-related shift in brain region activity during successful memory performance. Neurobiol Aging. 1998; 19(5):437–445. [PubMed: 9880046]

Johnson NA, Jahng GH, Weiner MW, Miller BL, Chui HC, Jagust WJ, Gorno-Tempini ML, Schuff N. Pattern of cerebral hypoperfusion in Alzheimer disease and mild cognitive impairment measured with arterial spin-labeling MR imaging: initial experience. Radiology. 2005; 234(3):851–859. [PubMed: 15734937]

Kawachi T, Ishii K, Sakamoto S, Matsui M, Mori T, Sasaki M. Gender differences in cerebral glucose metabolism: a PET study. J Neurol Sci. 2002; 199(1–2):79–83. [PubMed: 12084447]

Kohn MI, Tanna NK, Herman GT, Resnick SM, Mozley PD, Gur RE, Alavi A, Zimmerman RA, Gur RC. Analysis of brain and cerebrospinal fluid volumes with MR imaging. Part I. Methods, reliability, and validation. Radiology. 1991; 178(1):115–122. [PubMed: 1984289]

Kwong KK, Chesler DA, Weisskoff RM, Donahue KM, Davis TL, Ostergaard L, Campbell TA, Rosen BR. MR perfusion studies with T1-weighted echo planar imaging. Magn Reson Med. 1995; 34(6): 878–887. [PubMed: 8598815]

Maldjian JA, Laurienti PJ, Kraft RA, Burdette JH. An automated method for neuroanatomic and cytoarchitectonic atlas-based interrogation of fMRI data sets. Neuroimage. 2003; 19(3):1233–1239. [PubMed: 12880848]

Martin AJ, Friston KJ, Colebatch JG, Frackowiak RS. Decreases in regional cerebral blood flow with normal aging. J Cereb Blood Flow Metab. 1991; 11(4):684–689. [PubMed: 2050757]

Meltzer CC, Cantwell MN, Greer PJ, Ben-Eliezer D, Smith G, Frank G, Kaye WH, Houck PR, Price JC. Does cerebral blood flow decline in healthy aging? A PET study with partial-volume correction. J Nucl Med. 2000; 41(11):1842–1848. [PubMed: 11079492]

Miller SL, Celone K, DePeau K, Diamond E, Dickerson BC, Rentz D, Pihlajamaki M, Sperling RA. Age-related memory impairment associated with loss of parietal deactivation but preserved hippocampal activation. Proc Natl Acad Sci U S A. 2008; 105(6):2181–2186. [PubMed: 18238903]

Noth U, Meadows GE, Kotajima F, Deichmann R, Corfield DR, Turner R. Cerebral vascular response to hypercapnia: determination with perfusion MRI at 1.5 and 3.0 Tesla using a pulsed arterial spin labeling technique. J Magn Reson Imaging. 2006; 24(6):1229–1235. [PubMed: 17094105]

Parkes LM, Rashid W, Chard DT, Tofts PS. Normal cerebral perfusion measurements using arterial spin labeling: reproducibility, stability, and age and gender effects. Magn Reson Med. 2004; 51(4): 736–743. [PubMed: 15065246]

Relihac A, Rousset OG, Comtat C, Frouin V, Gregoire MC, Evans AC. A correction algorithm for patial volume effects in 3D PET Imaging: Principle and Validation. IEEE. 2001:18–62.

Restom K, Bangen KJ, Bondi MW, Perthen JE, Liu TT. Cerebral blood flow and BOLD responses to a memory encoding task: a comparison between healthy young and elderly adults. Neuroimage. 2007; 37(2):430–439. [PubMed: 17590353]

Schmidt K, Sokoloff L. A computationally efficient algorithm for determining regional cerebral blood flow in heterogeneous tissues by positron emission tomography. IEEE Trans Med Imaging. 2001; 20(7):618–632. [PubMed: 11465468]

Stern Y, Zarahn E, Habeck C, Holtzer R, Rakitin BC, Kumar A, Flynn J, Steffener J, Brown T. A common neural network for cognitive reserve in verbal and object working memory in young but not old. Cereb Cortex. 2008; 18(4):959–967. [PubMed: 17675368]

Tanna NK, Kohn MI, Horwich DN, Jolles PR, Zimmerman RA, Alves WM, Alavi A. Analysis of brain and cerebrospinal fluid volumes with MR imaging: impact on PET data correction for atrophy. Part II. Aging and Alzheimer dementia. Radiology. 1991; 178(1):123–130. [PubMed: 1984290]

Wang J, Alsop DC, Li L, Listerud J, Gonzalez-At JB, Schnall MD, Detre JA. Comparison of quantitative perfusion imaging using arterial spin labeling at 1.5 and 4.0 Tesla. Magn Reson Med. 2002; 48(2):242–254. [PubMed: 12210932]

Werner R, Norris DG, Alfke K, Mehdorn HM, Jansen O. Improving the amplitude-modulated control experiment for multislice continuous arterial spin labeling. Magn Reson Med. 2005; 53(5):1096–1102. [PubMed: 15844087]

Wiersma J, Deichmann R, Ordidge R, Turner R. Removing the effects of CSF partial voluming on fitted CBF and arterial transit times using FAIR, a pulsed arterial spin labelling technique. Magma. 2006; 19(3):115–123. [PubMed: 16763807]

Ye FQ, Berman KF, Ellmore T, Esposito G, van Horn JD, Yang Y, Duyn J, Smith AM, Frank JA, Weinberger DR, et al. H(2)(15)O PET validation of steady-state arterial spin tagging cerebral blood flow measurements in humans. Magn Reson Med. 2000; 44(3):450–456. [PubMed: 10975898]
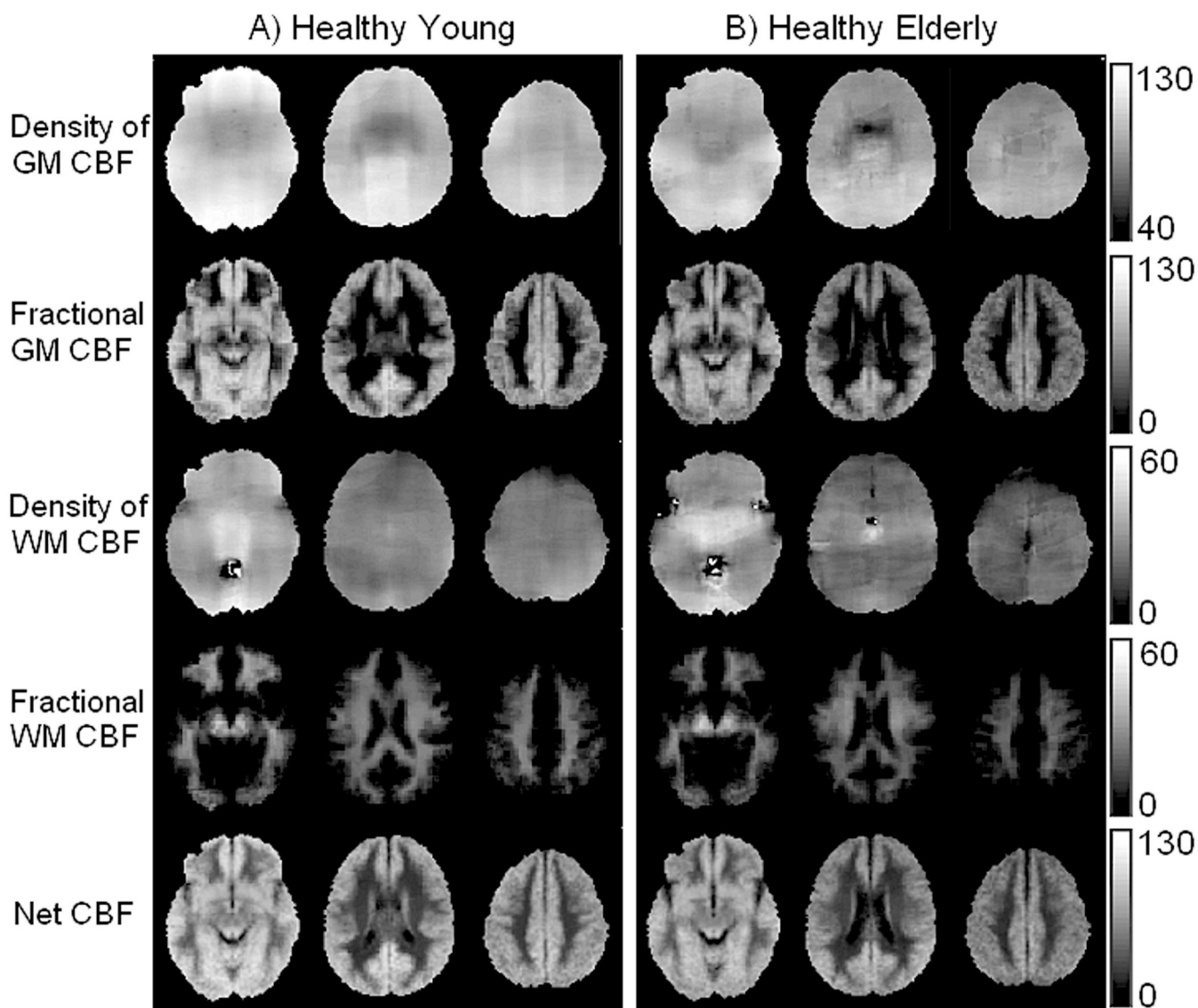
Fig. 1.
Group averaged CBF images from HY (A) and HE (B). 1st and 3rd rows show tissue specific images, f_{GM} and f_{WM}, respectively. Fractional CBF images, f_{GM}^{P} and f_{WM}^{P} for are shown in 2nd and 4th rows, respectively; the last row shows f_{NET}. Slices were chosen to represent lower, middle, and upper areas of the brain (MNI z-coordinates: 21, 37, 41). Units in the bars are in mL/100g min. Note good uniformity of the image signal for GM and WM flow densities (1st and 3rd rows).
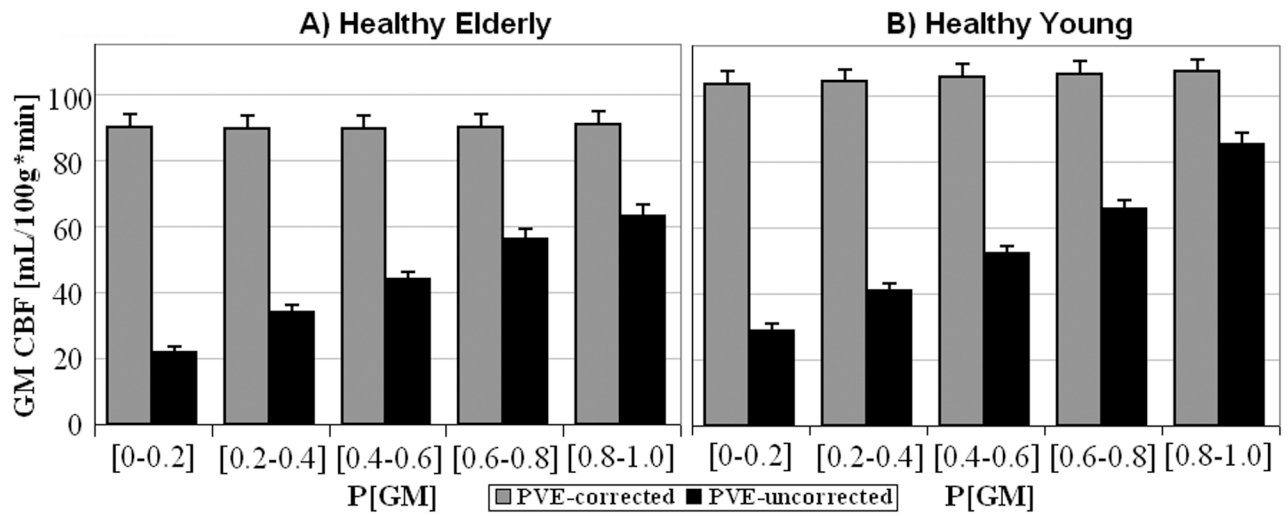
Fig. 2.
Pure GM CBF values from PVE-corrected data (grey) and uncorrected data (black) from HE (A) and HY (B). ROIs were selected to contain voxels with varying GM content from (0–20%) to (80–100%). Error bars represent + 1 s.e.
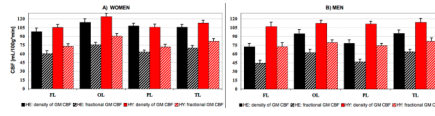
Fig. 3.

Lobewise f_{GM} and f_{GM}^P for women (A) and men (B), respectively. GM flow density is shown in solid for HY and striped blue for HE, while the solid and striped red represent the fractional CBF for HY and HE, respectively. Error bars represent +1 s.e.
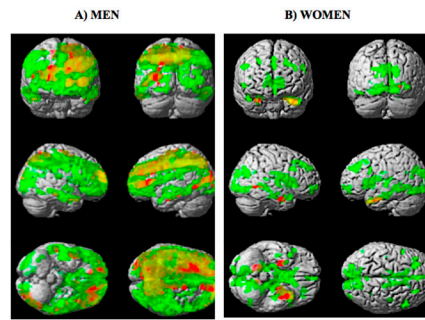
Fig. 4.
Voxelwise SPM{T}map for the (HY - HE) contrast (corrected at the cluster level of 50 voxels, T > 3.84) overlaid on a surface rendering of the brain for females (A) and males (B) for f_{GM} (red) and f_{NET} (green). The overlap of the areas where both f_{GM} and f_{NET} were statistically lower in HE are shown in orange.
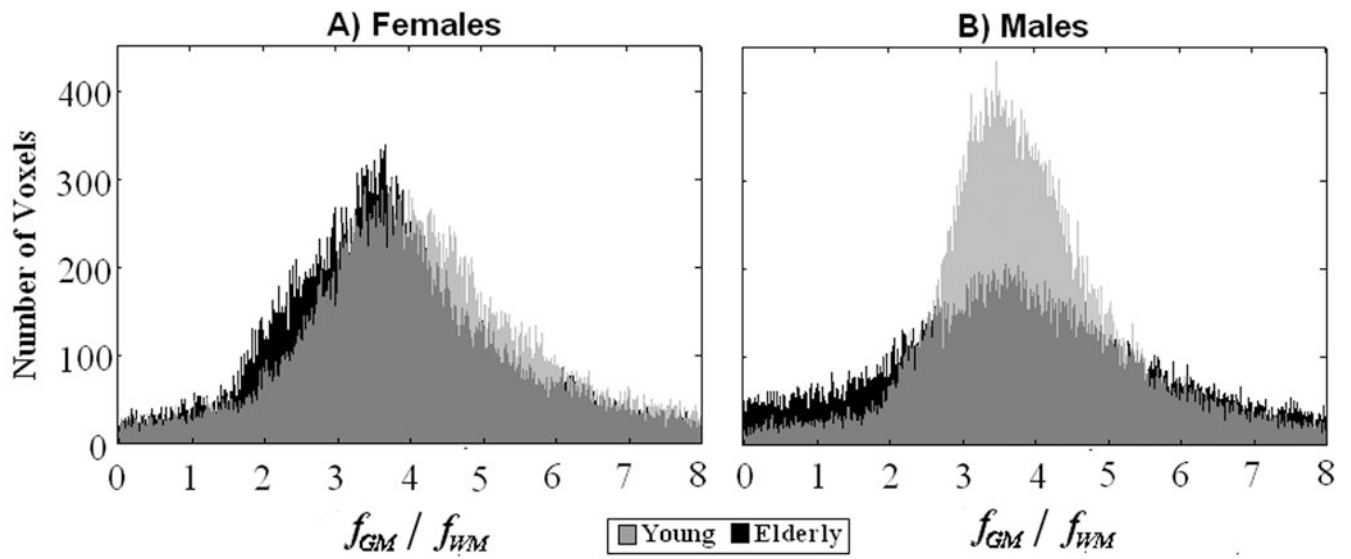
Fig. 5.

Histograms of whole brain ratios of f_{GM}/f_{WM} for females (A) and males (B) are shown in black and grey for HY and HE, respectively.